Supporting Information

Rapid capture of trace precious metals by amyloid-like protein membrane with high adsorption capacity and selectivity

Facui Yang,[1, a] Zhigang Yan,[1, b] Jian Zhao,[a] Shuting Miao,[a] Dong Wang,[c] and Peng Yang,*[, a]

[*] Corresponding authors: P. Yang, E-mail: yangpeng@snnu.edu.cn

[1] Facui Yang and Zhigang Yan contributed equally to this work.

[a] Key Laboratory of Applied Surface and Colloid Chemistry, Ministry of Education, School of Chemistry and Chemical Engineering, Shaanxi Normal University, Xi'an 710119, China, E-mail: yangpeng@snnu.edu.cn.

[b] Department of Orthopaedics, Beijing Longfu Hospital, Beijing 100010, China.

[c] School of Mechanical and Precision Instrument Engineering, Xi'an University of Technology, Xi'an 710048, China.

1. Experimental Section

1.1. Materials.

Lysozyme was purchased from Sigma-Aldrich. Tris (2-carboxyethyl) phosphine hydrochloride (TCEP) was purchased from TCI. Hydrochloric acid (36%~38% HCl), nitric acid (68% HNO_3), sodium hydroxide (NaOH) and sulfuric acid (98% H_2SO_4) were purchased from Sinopharm Chemical. HEPES (4-(2-hydroxyethyl)-1-piperazineethanesulfonic acid) buffer (pH = 7.2~7.4) was obtained from Solarbio. Thiourea (CH_4N_2S), ammonium thiocyanate (NH_4SCN), chloroauric acid ($HAuCl_4$), all Inductively Coupled Plasma Mass Spectrometry (ICP-MS) standard solutions (1000 ppm of Pd, Pt, Rh, Ir, Ru or Os in 2 M HCl, 1000 ppm of Ag in 1% HNO_3) were purchased from Aladdin. Ferric sulfate ($Fe_2(SO_4)_3$) was purchased from Macklin. Ultrapure water was used in all experiments and was supplied by Milli-Q Advantage A10 (Millipore, USA). Original gold ore powder (nominally 200 mesh) was obtained from Jiangxi province, China. Mobile phone chips were acquired from waste phone (Huawei, Motorola, Samsung). Track-Etched polyethylene terephthalate (PET) nuclepore membranes (a pore size distribution at 10 μm) were purchased from Wuwei Kejin Xinfa technology Co. Ltd. (Gansu, China).

1.2. Characterization.

X-ray photoelectron spectroscopy (XPS) was performed with AXIS Ultra from Kratos Analytical Ltd. (Japan), and the binding energies were calibrated by setting the C1s peak at 284.6 eV. Scanning electron microscopy (SEM) analyses were carried out using a field emission scanning electron microscope (FE-SEM) (SU8020, Hitachi) at an acceleration voltage of 1 kV. Gold structure and morphology were characterized by field emission transmission electron microscopy (FE-TEM) (Tecnai G2 F20) at 200 kV without staining. The BET surface area was acquired through nitrogen absorption-desorption on a surface aperture adsorption instrument (ASAP2020, Micromeritics, USA). Inductively coupled plasma mass spectrometry (ICP-MS, aurora M90, Bruker, USA) was utilized to measure the concentration of Au and other metals. The samples, filtered through a 0.22 μm membrane filter, were diluted with ultrapure 1% HNO3 and analyzed for contents of metal ions by comparison with standard solutions.

1.3. Preparation of the bilayer PTL membrane.

The lysozyme phase-transition buffer was freshly prepared by mixing a stock buffer solution of lysozyme (30 mg mL^{-1} in 10 mM HEPES buffer at pH 7.0) with TCEP buffer (50 mM TCEP in 10 mM HEPES buffer at pH 7.0, pH adjusted with 5 M NaOH) at a volume ratio of 1:1. The protein phase-transition buffer was dropped on a piece of glass (e.g., 24×24 mm). Then, the solution on the substrate was incubated in a humid environment (generally for ~120 min) at room temperature. The phase transition of lysozyme was initiated spontaneously upon mixing, and the PTL product was deposited on the surface of glass. Then, the PTL product was cross-linked by submerging the glass

in 1 wt% aqueous glutaraldehyde for 30 min and rinsing it in water. Then, the membranes were detached from the glass in a 1 M NaOH solution. These membranes were then used to adsorb precious metal ions from the acidic aqueous solution of single or mixed metal ions.

2. Adsorption performance of Au^{3+}.

2.1. Adsorption kinetics.

The adsorption procedure was similar to that of the adsorption isotherm study, but the concentration of Au^{3+} ($HAuCl_4$) was analyzed at regular intervals by ICP-MS during the adsorption process. The adsorption capacity at time t (min) was obtained by mass balance calculation and was denoted as q_t (mg g^{-1}). The adsorption ratio (R_A) was calculated by the difference in the metal ion equilibrium concentration before and after adsorption (see Equation (1)).

$$R_A = \frac{C_0 - C_e}{C_0} \times 100\% \quad (1)$$

2.2. Adsorption isotherm.

Adsorption experiments were carried out in 5 mL solutions with initial Au^{3+} ($HAuCl_4$) concentrations ranging from 196.9 to 984.8 ppm by diluting 29.4 mM $HAuCl_4$ aqueous solution. The pH of the solutions was adjusted to 3.0 with HCl, and the PTL membrane was suspended in the gold ion solution. Then, adsorption experiments were conducted for 24 h at 283, 310 and 333 K. The concentration of Au^{3+} after attaining adsorption equilibrium was analyzed by ICP-MS, and the adsorption capacity was calculated according to Equation (2).

$$q_e = \frac{V(C_0 - C_e)}{m} \quad (2)$$

where C_0 and C_e represent the initial and equilibrium Au^{3+} concentrations (ppm), respectively. V is the volume of Au^{3+} solution (L), and m is the dosage of the membrane (g).

2.3. Adsorption of precious metal ions.

For the adsorption of single precious metals (Ag, Pd, Pt, Ir, Os, Ru and Rh), adsorption experiments were carried out in 5 mL 1% HNO_3 solution with an initial concentration ranging from 1 to 500 ppm by diluting precious metal standard solution (1000 ppm of Pd, Ir, Os, Pt, Ru or Rh in 2 M HCl). Silver can precipitate in the presence of chloride, so the corresponding standard solution was 1000 ppm of Ag in 1% HNO_3 solution.

For the adsorption of mixed precious metals (Pd, Pt, Ir, Os, Ru and Rh), adsorption experiments were carried out in 5 mL 1% HNO_3 solution with an initial concentration ranging from 0.5 to 50 ppm by diluting precious metal standard solution (Pd, Pt, Rh, Ir, Ru and Os in 2 M HCl).

The effect of anions on gold adsorption: adsorption experiments were carried out in 5 mL 0.01 M HCl, 0.01 M HNO_3 or 0.01 M H_2SO_4 solution with an initial concentration of Au^{3+} ($HAuCl_4$) of 393.9 ppm.

2.4. Gold leaching from gold ores or mobile phone chips.

First, a method was developed to guarantee the complete dissolution of all metals contained in gold ores or mobile phone chips. This purpose was achieved by preparing and using aqua regia solution (concentrated HCl: concentrated HNO_3 = 3:1 v/v). Typically, in a 50 mL round-bottom flask with a three-way valve, 1 g of gold ore powder was added to 20 mL of aqua regia with stirring at 300 rpm. For electronic waste, in a 250 mL glass bottle with a lid, 80 g of a mobile phone chip was added to 100 mL of aqua regia. After the reaction was completed at a determined time, the leaching solution was passed through a 0.22 μm membrane filter. Finally, the weight percentage of each metal component contained in the gold ore or mobile phone chip was directly quantified by analyzing the leaching solution via ICP-MS.

2.5. Adsorption-desorption and recovery of gold from the adsorbed membrane.

In order to reuse the membrane more easily, the bottom nanomembrane layer of the PTL adsorbent could be adhered onto a PET nuclear pore membrane (PTL/PET), which was used for the circulation adsorption studies. The adsorption of Au^{3+} were then carried out by flowing 40 mL mixed metal ions solution (Au^{3+}, Zn^{2+}, Mg^{2+}, Cu^{2+}, Ni^{2+}, Sn^{2+}, Fe^{3+}, Co^{2+}, Al^{3+}, Cr^{3+}, Bi^{2+}, Sb^{2+}, Se^{4+} and Li^{+}) solution through the PTL/PET membrane via peristaltic pump cycling (NEW KCP, Kamoer, China) at a flow rate of 5 mL/min for 3 h (Fig. 6a). The desorption of Au from the PTL/PET membrane was then achieved by immersing the membrane in an eluent solution of a combination of thiourea (130 mM), ammonium thiocyanate (780 mM), and ferric sulfate (28 mM) for 12 h at room temperature, followed by the ICP-MS test on the solution.

Gold leaching from membrane by N-bromosuccinimide (NBS) and pyridine (Py) method. The Au-PTL membranes were added to 10 ml of NBS/Py solution at pH 8.0 for 12 h. The original dosage for each chemical combination was at 10/100 mM for NBS/Py.

The recovery of gold from the eluent solutions was performed by adding sodium borohydride (2 mg mL^{-1}) and continuously agitating for 30 min at room temperature to give reduced gold metal as a precipitate. After filtration, the concentration of Au in the filtrate was determined by ICP-MS to calculate the recovery ratio of gold from the membrane. Alternatively, to obtain gold with high purity, the gold-loaded PTL was incinerated to remove organic constituents and directly recover the gold from the Au-loaded PTL in the form of gold powder (23 K) after pyrolysis of the sample at 900 °C for 5 h Materials.

Supporting Figures：

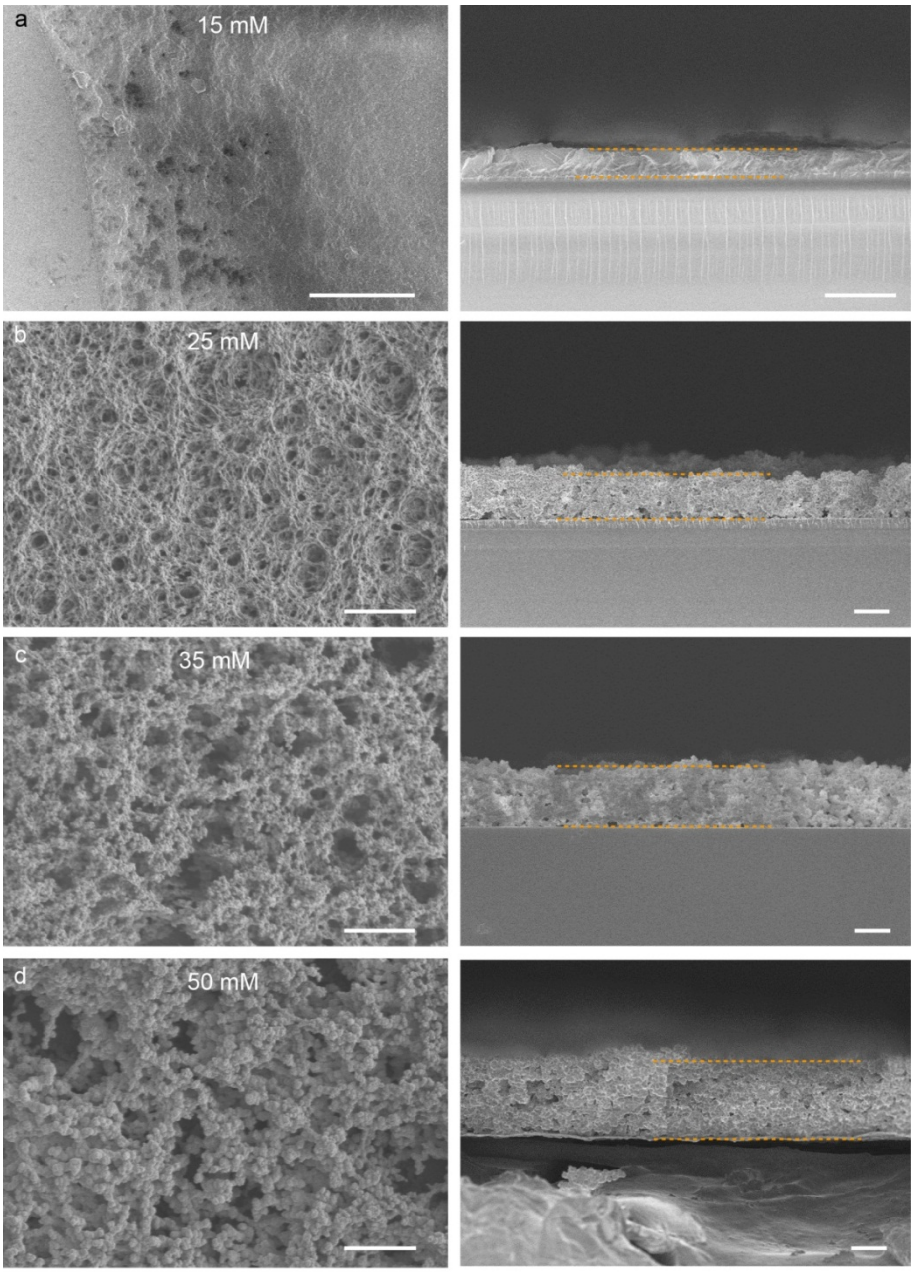

Figure S1. SEM images to show the surface (left) and thickness (right) of the PTL bilayer membrane with the concentration of TCEP buffer at 15 (a), 25 (b), 35 (c) and 50 mM (d), respectively. Scale bars were 10 μm.

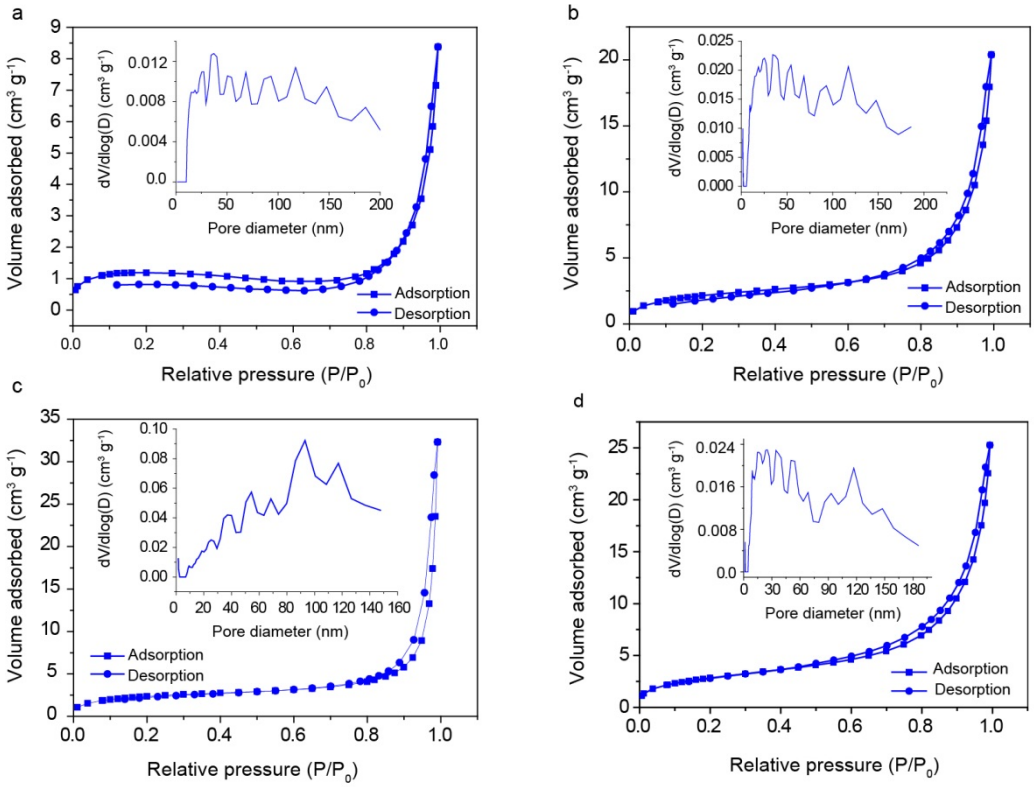

Figure S2. Nitrogen adsorption-desorption isotherms and corresponding pore size distributions for the membrane at 15 (a), 25 (b), 35 (c) and 50 mM TCEP (d), respectively. For other given conditions: the concentration of lysozyme was 30 mg mL^{-1}, pH 7.0 of TCEP buffer and incubation for 12 h. The Brunauer-Emmett-Teller (BET) specific surface area of the membranes was 3.6 m^2 g^{-1} (15 mM), 7.8 m^2 g^{-1} (25 mM), 8.4 m^2 g^{-1} (35 mM) and 10.5 m^2 g^{-1} (50 mM), respectively.

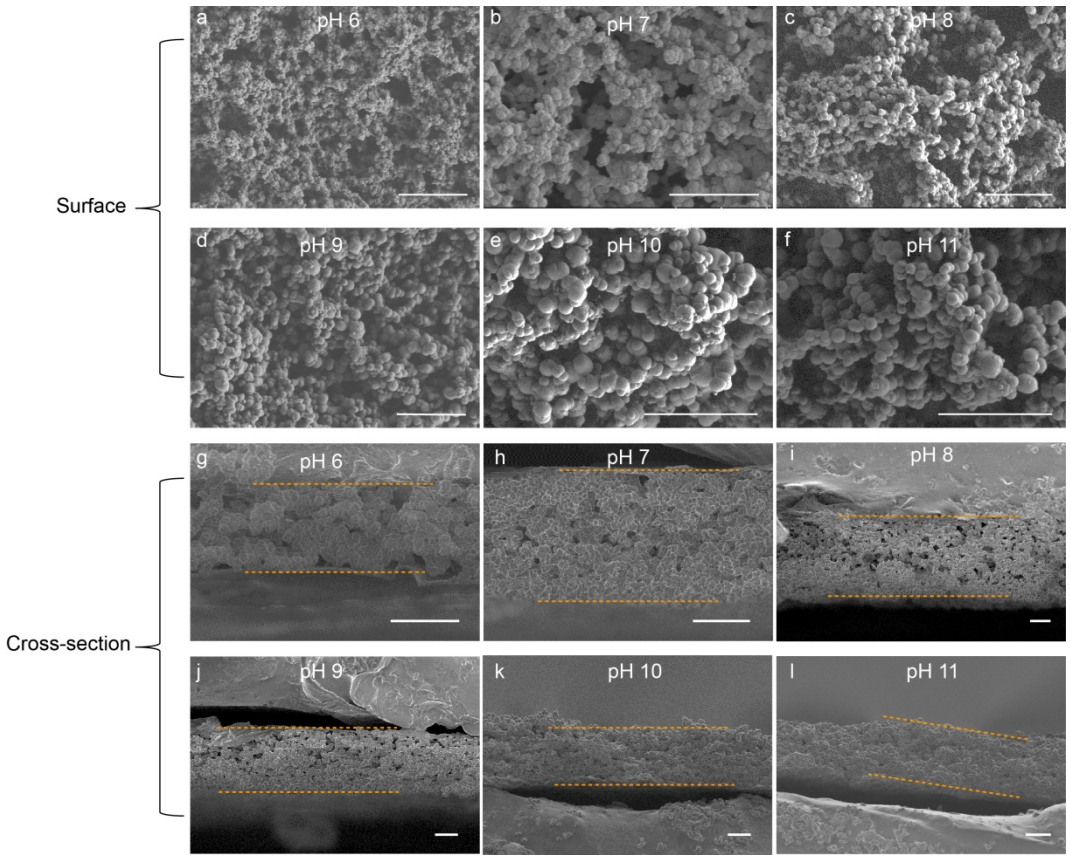

Figure S3. (a-f) SEM images to show the PTL bilayer membrane with the pH of TCEP buffer at 6, 7, 8, 9, 10, 11, respectively. (g-l) SEM images showing the cross-section of the PTL bilayer membrane with the pH of TCEP buffer at 6, 7, 8, 9, 10, 11, respectively. The concentration of lysozyme was 30 mg mL^{-1}. Scale bars were 10 μm.

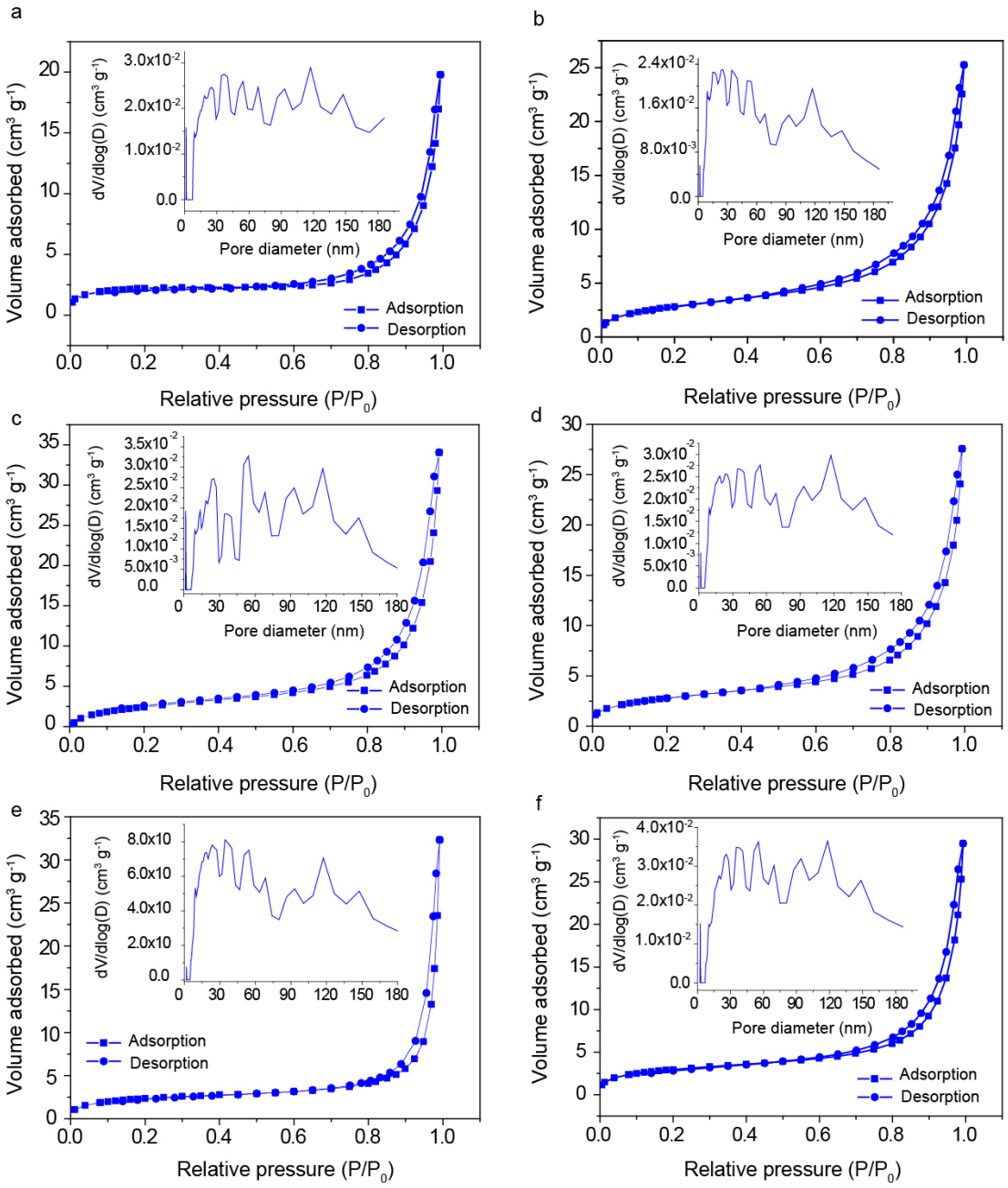

Figure S4. Nitrogen adsorption-desorption isotherms and corresponding pore size distributions for the membrane with the pH of TCEP buffer at (a) 6, (b) 7, (c) 8, (d) 9, (e) 10, (f) 11, respectively. For other given conditions: the concentration of lysozyme was 30 mg mL^{-1}, and 50 mM of TCEP buffer. The BET specific surface area of the membranes was 7.4 m^2 g^{-1} (pH 6), 10.5 m^2 g^{-1} (pH 7), 10.3 m^2 g^{-1} (pH 8), 10.1 m^2 g^{-1} (pH 9), 10.2 m^2 g^{-1} (pH 10) and 10.6 m^2 g^{-1} (pH 11), respectively.

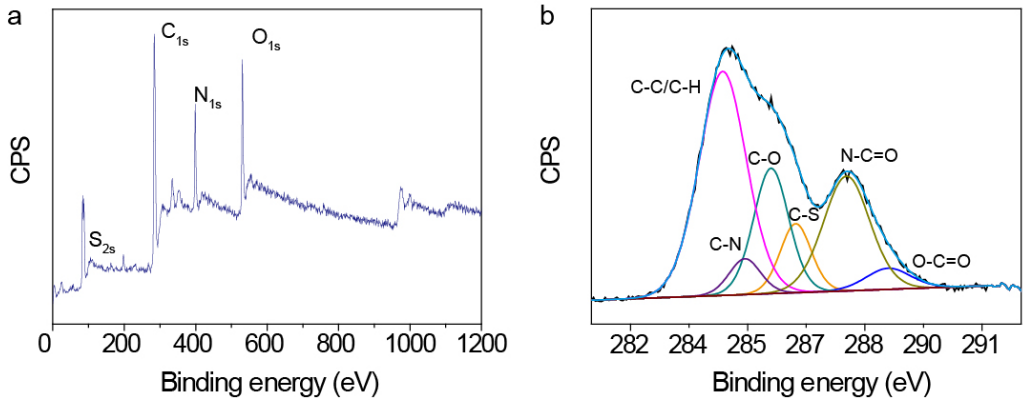

Figure S5. (a) XPS survey characterization on the cross-linked PTL bilayer membrane. (b) High-resolution C_{1s} spectra of the cross-linked PTL bilayer membrane. The deconvolution of C_{1s} peak indicated that the membrane surface presented multiple functional groups mainly including alphatic carbon (C-H/C-C), amines (C-N), hydroxyls (C-O), thiols (C-S), amides (O=C-N) and carboxyl groups (O=C-O).

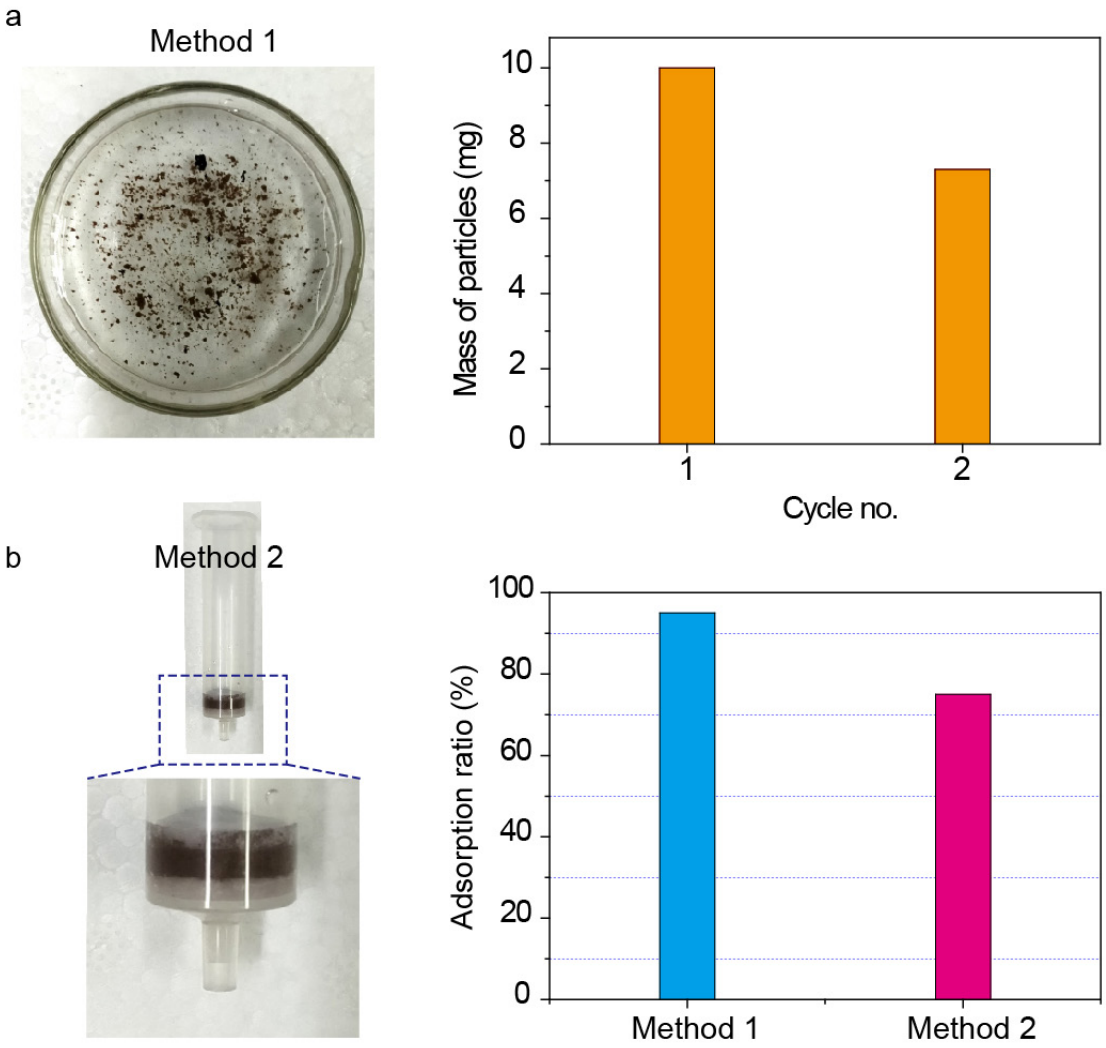

Figure S6. (a) The microparticles dispersed in the gold ion solution as adsorbents (Method 1) and the recovered mass of microparticles for the gold adsorption at first and second time. (b) Photograph of the microparticles as fillers for the adsorption column (Method 2), and the adsorption ratio of gold ions for the microparticles by using method 1 and method 2.

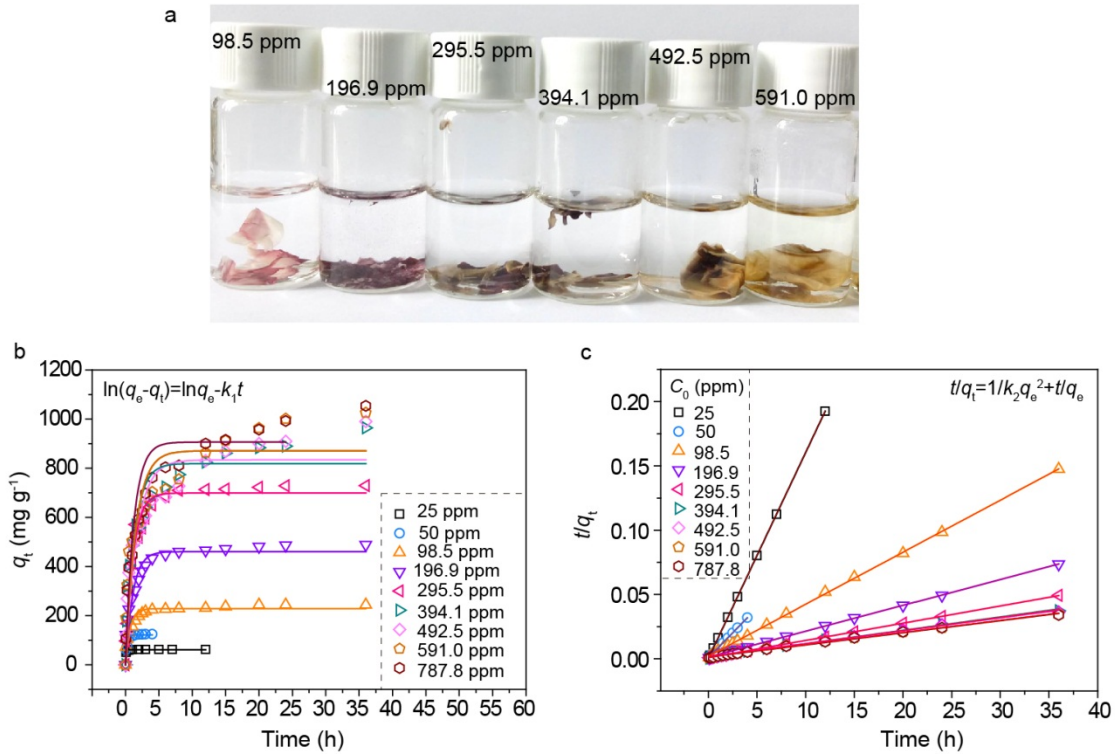

Figure S7. (a) The photograph of the solution after the PTL bilayer membrane (dispersed in the solution) adsorbing gold ions at different concentration. Adsorption kinetics at (b) the pseudo-first-order and **c,** pseudo-second-order, to fit the gold ion adsorption on the PTL bilayer membrane at 310 K. Obviously, the pseudo-second-order kinetics fitted the data better than that for the pseudo-first-order.

The adsorption kinetics gold ions of on the membrane was analyzed by applying the pseudo-first-order and pseudo-second-order kinetic models to fit the experimental data, expressed respectively as:

$$\ln(q_e - q_t) = \ln q_e - k_1 t \qquad (1)$$

$$t/q_t = 1/(k_2 \cdot q_e^2) + t/q_e \qquad (2)$$

where q_t and q_e (mg/g) are the amounts of metal ions adsorbed per unit mass of the adsorbent at time t and at equilibrium, k_1 (h^{-1}) is the first order rate constant of adsorption, k_2 (g mg^{-1} h^{-1}) is the rate constant of adsorption equilibrium in the second order reaction. The relative values calculated from the two models were listed in Table S1.

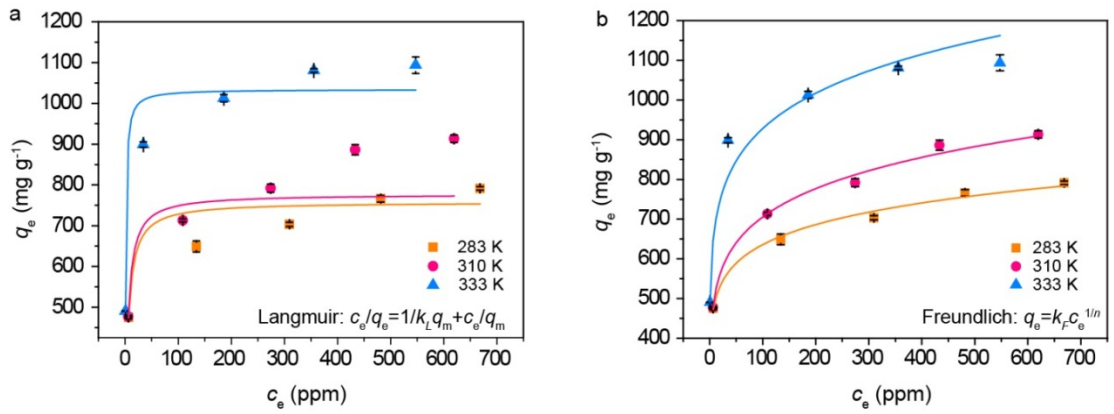

Figure S8. Adsorption isotherm for (a) Langmuir and (b) Freundlich model to fit the gold ion adsorption on the PTL bilayer membrane at three different temperatures, respectively. The other conditions: pH = 3.0, initial gold ion concentration was 196.9-984.8 ppm. Obviously, the Freundlich model fitted the data better than that for the Langmuir model.

The equilibrium sorption experimental data obtained in this study were analyzed using the commonly used Langmuir (3) and Freundlich isotherm (4).

$$c_e/q_e = c_e/q_m + 1/(q_m \cdot k_L) \quad (3)$$

$$q_e = k_F \cdot c_e^{1/n} \quad (4)$$

where c_e is the equilibrium concentration of metal ions remained in the solution (ppm); q_e is the amount of metal ions adsorbed on per weight unit of solid after equilibrium (mg g^{-1}); q_m, the maximum adsorption capacity, is the amount of adsorbate at complete monolayer coverage (mg g^{-1}), and k_L (L mg^{-1}) is a constant that relates to the heat of adsorption. k_F and n are Freundlich constants which are related to adsorption capacity and intensity of adsorption. Furthermore, the Langmuir parameters can be used to predict if the adsorption is favorable or not. A dimensionless separation factor of R_L from k_L, which is defined as $R_L = 1/(1 + k_L C_0)$, shows that if $0 < R_L < 1$, the adsorption is favorable, if $R_L = 1$, the adsorption is linear, if $R_L > 1$, the adsorption is unfavorable, and if $R_L = 0$, the adsorption is irreversible. On average, a favorable adsorption tends to have Freundlich constant n between 1 and 10. Larger value of n (smaller value of $1/n$) implies stronger interaction between the adsorbent and ions while $1/n$ equal to 1 indicates linear adsorption leading to identical adsorption energies for all sites. The relative values calculated from the two models were listed in Table S2.

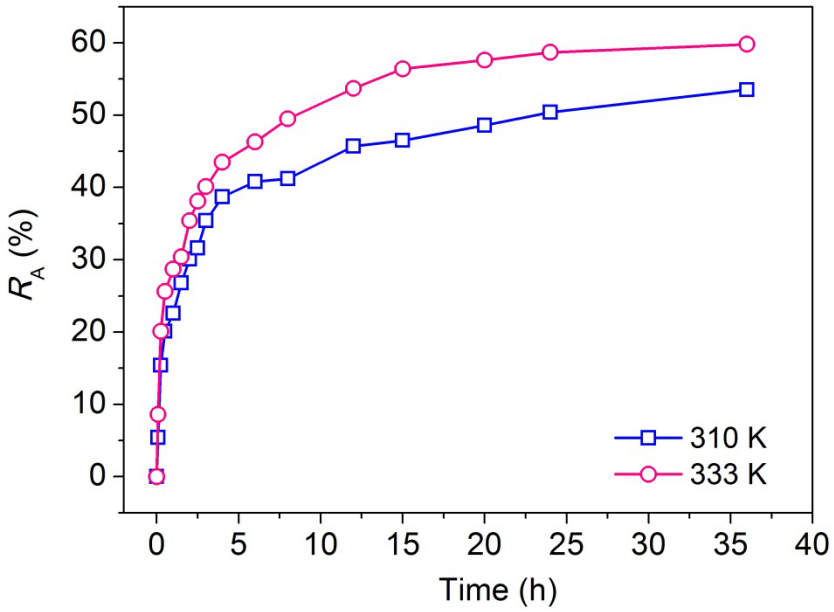

Figure S9. Time-dependent gold adsorption ratio at the initial gold ion concentration being 787.8 ppm with pH 2.5 at 310 K and 333 K, respectively.

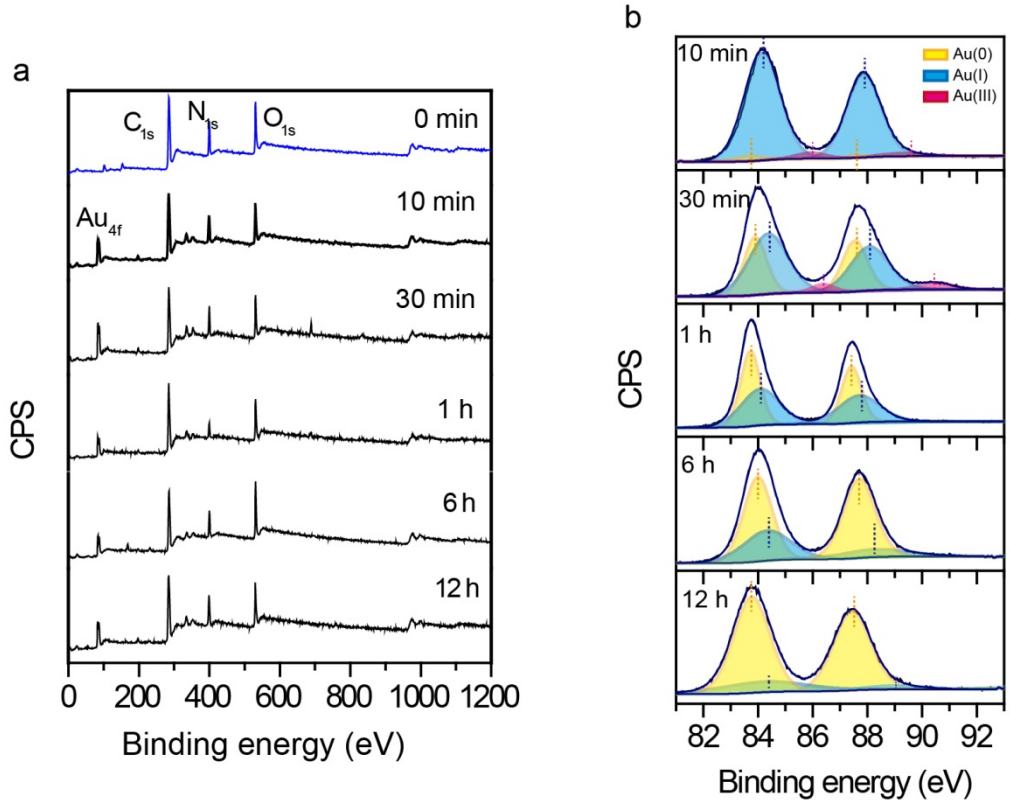

Figure S10. (a) X-ray photoelectron spectroscopy (XPS) wide scan on the membrane after the gold adsorption to show the gold characteristic peaks at different adsorption time. (b) Deconvolution of high-resolution XPS spectra of Au_{4f} of the PTL bilayer membrane after adsorbing gold ions.

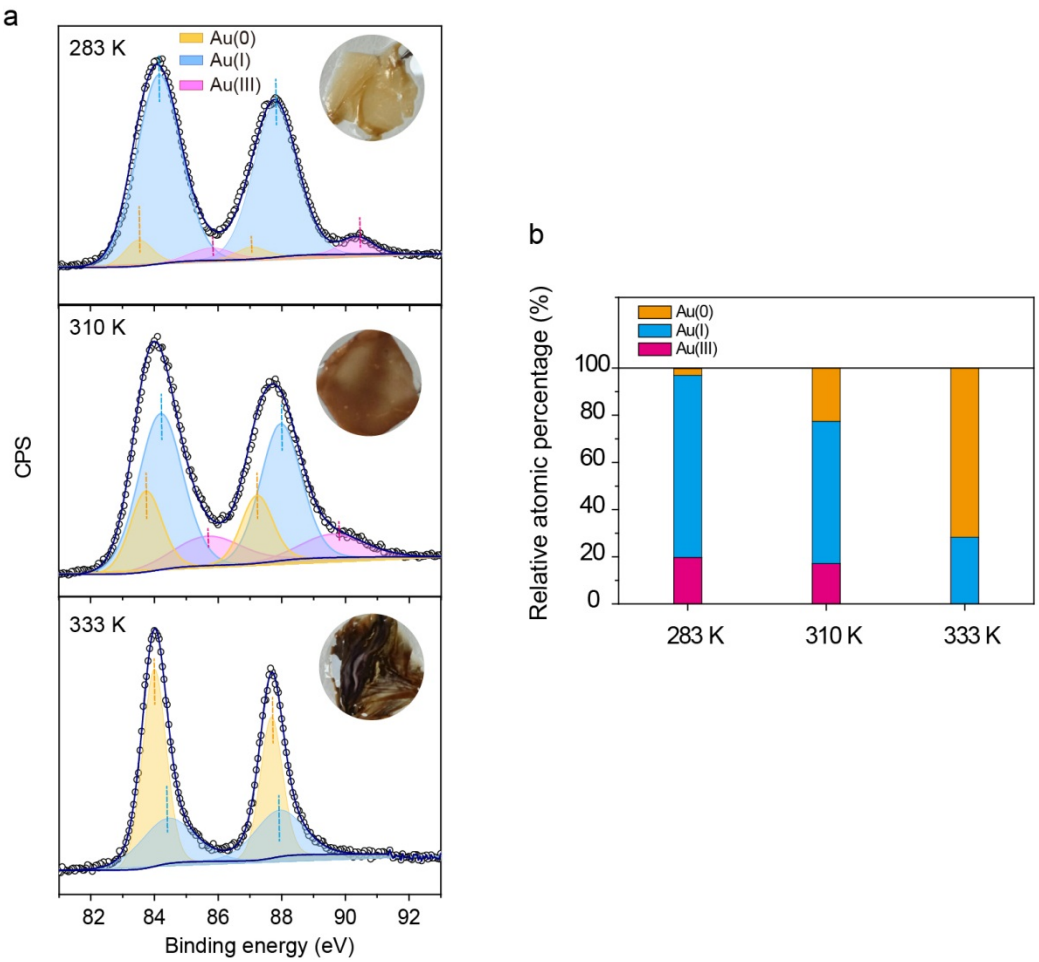

Figure S11. (a) Deconvolution of high-resolution XPS spectra of Au_{4f} on the PTL bilayer membrane after adsorbing $[AuCl_4]^-$ within 1 h at different temperature (283, 310 and 333 K), and the inset image was the photograph of the membrane after adsorbing gold ions. (b) Relative atomic percentage representing atomic fractions per total Au content for Au(III), Au(I) and Au(0) at different temperature from the XPS spectra of Au_{4f}.

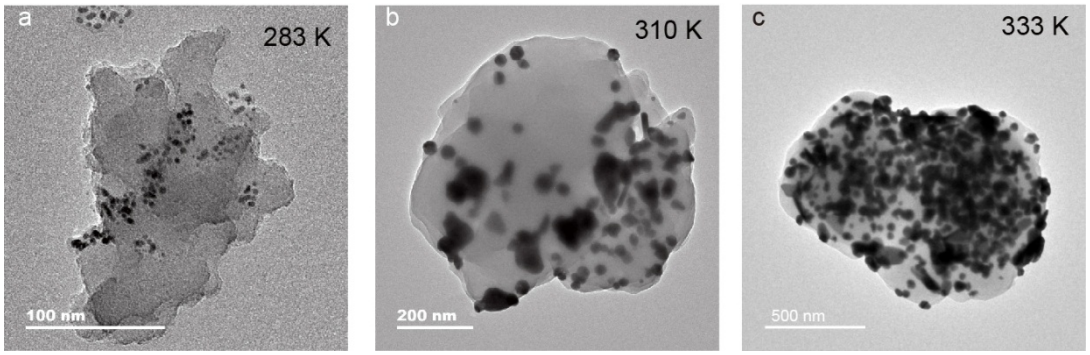

Figure S12. The TEM images of a piece of the PTL bilayer membrane after adsorbing gold ions at (a) 283 K, (b) 310 K and (c) 333 K temperature, respectively.

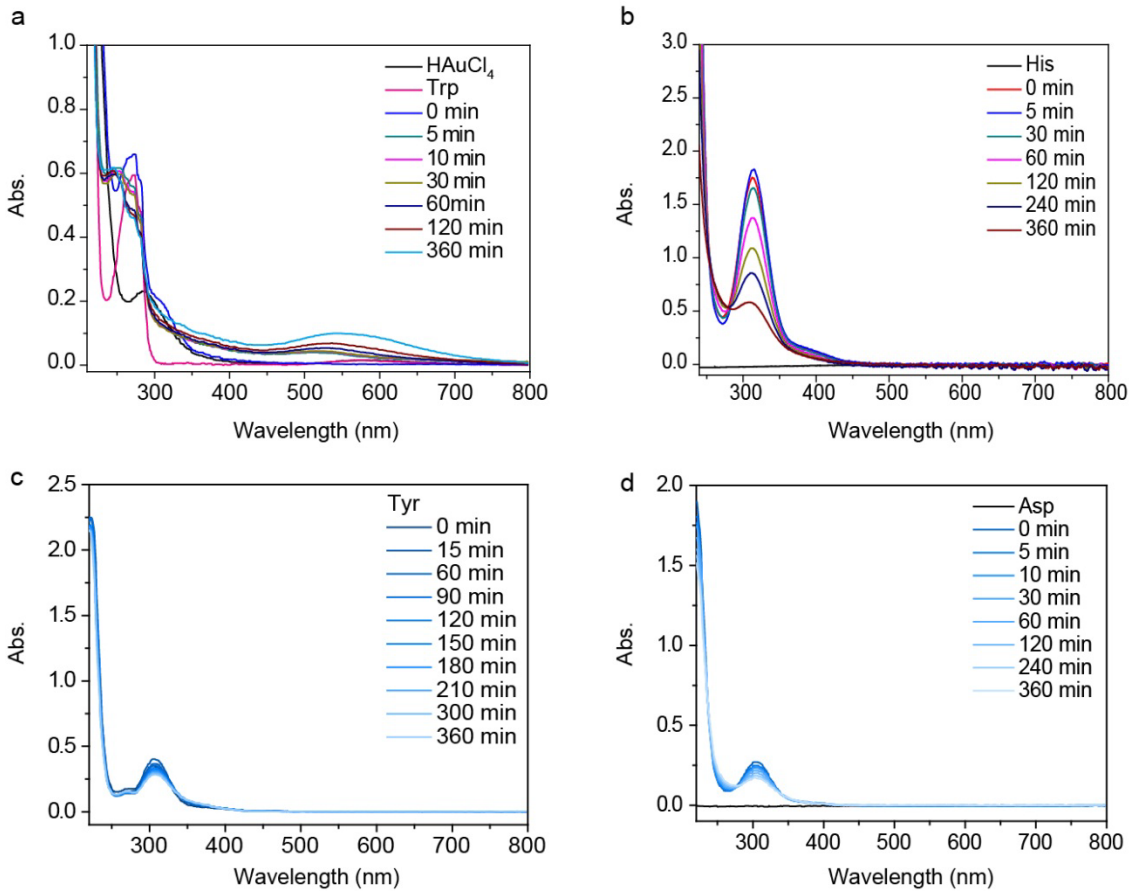

Figure S13. (a-d) Reduction of 1 mM chloroauric acid by 0.1 mM (a) tryptophan (Trp), (b) histidine (His), (c) tyrosine (Tyr) and (d) aspartic acid (Asp), respectively, as recorded by the UV/vis spectra of the chloroauric acid solution after the addition of amino acids at different time.

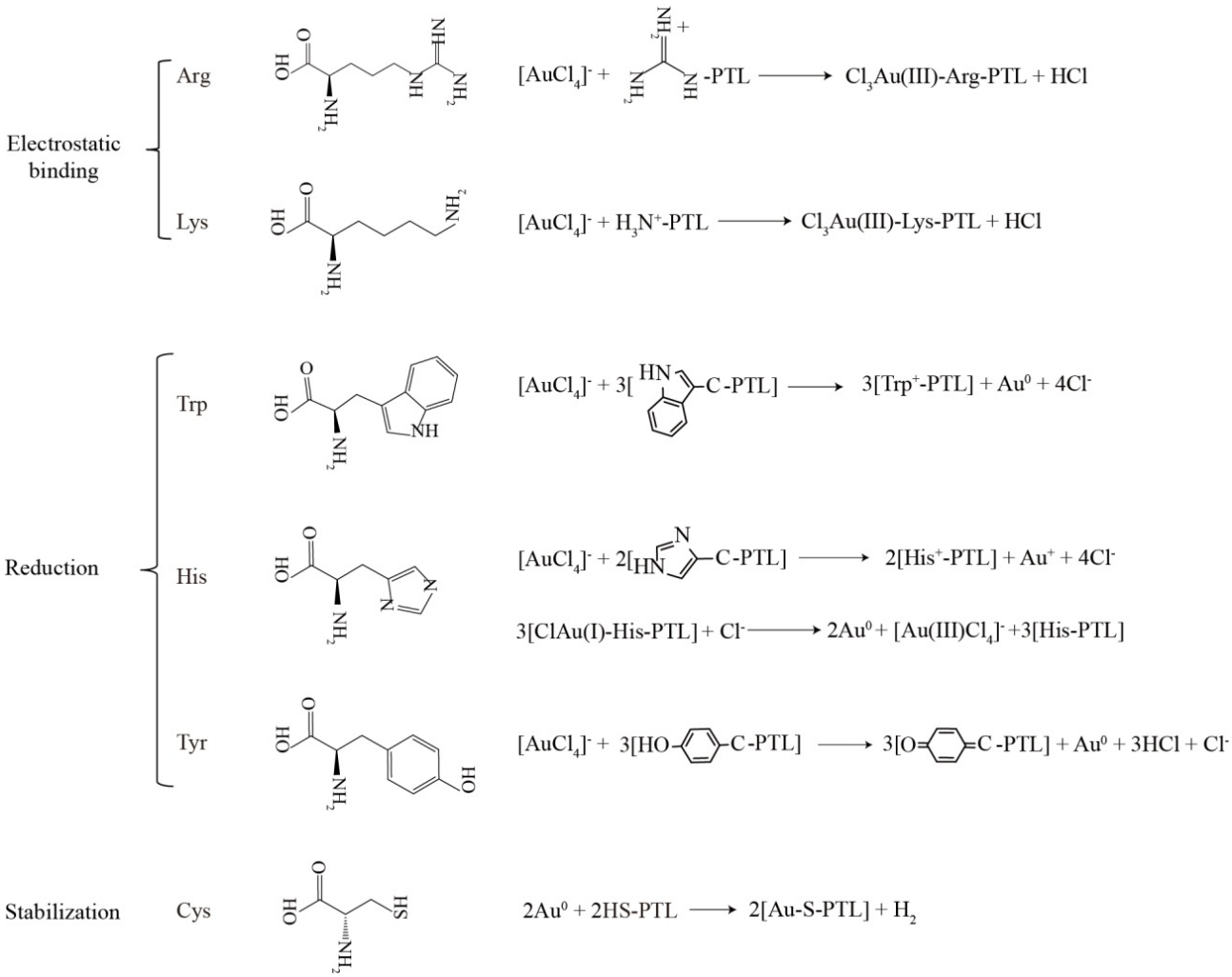

Figure S14. The adsorption and reduction reactions of gold ions on the PTL bilayer membrane. Arg: arginine; Lys: lysine; Trp: tryptophan;[1, 2] His: histidine;[3] Tyr: tyrosine; Cys: cysteine.[4]

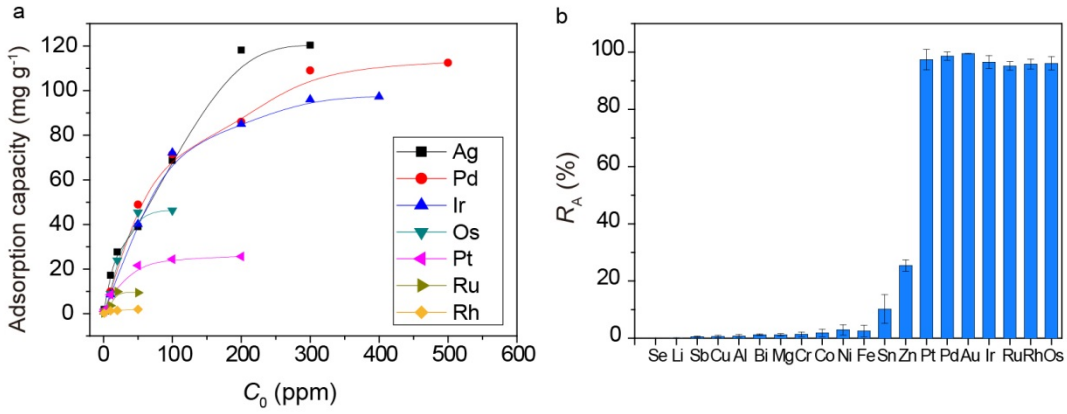

Figure S15. (a) Adsorption capacity of the PTL bilayer membrane for single precious metal (Ag, Pd, Pt, Ir, Os, Ru and Rh) at different initial concentration C_0. (b) The effect of competing metal ions (1 ppm each) on precious metal ions adsorption.

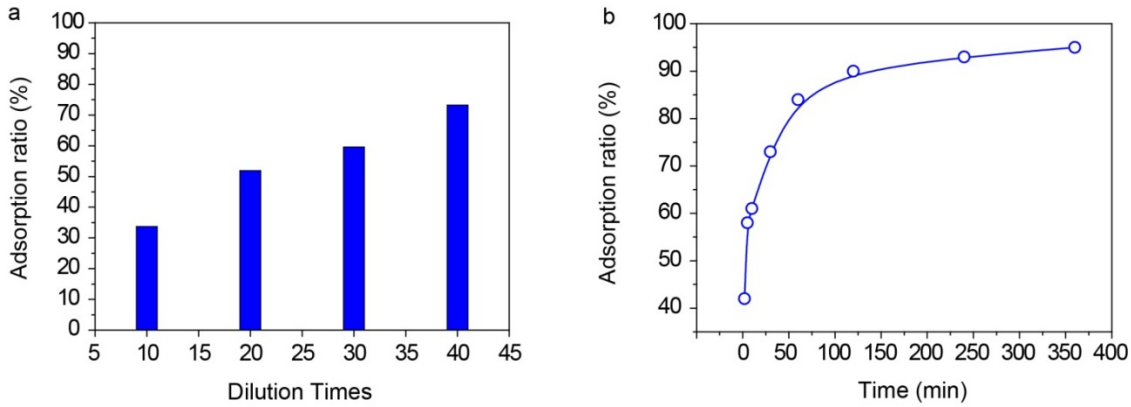

Figure S16. (a) The adsorption ratio of gold ions on the PTL bilayer membrane from the aqua regia leaching solution of gold ores at different dilution times. (b) The adsorption ratio of gold ions on the PTL bilayer membrane at different time in the 40 mL aqua regia leaching solution (dilution 40 times) from the gold ores.

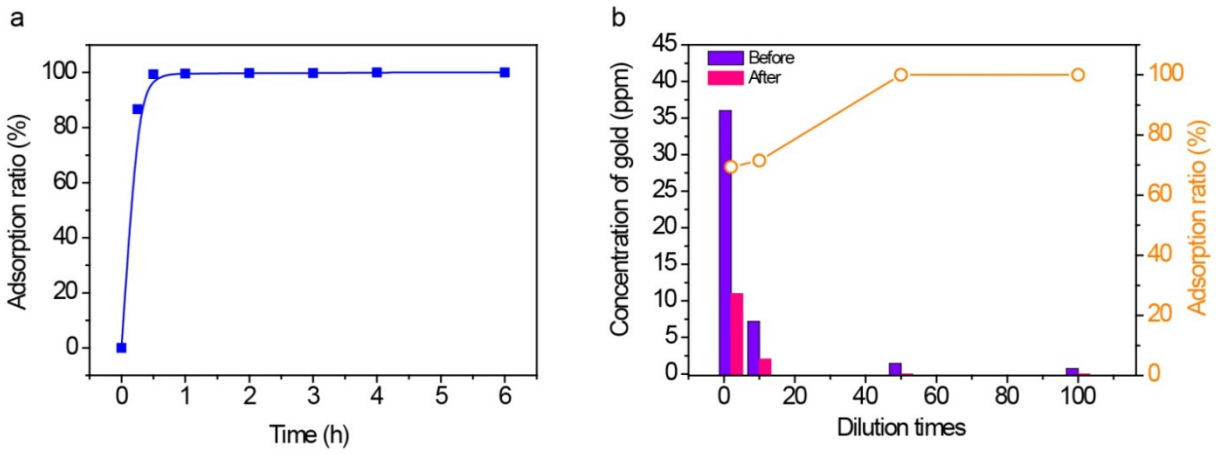

Figure S17. (a) The adsorption ratio of gold ions on the PTL bilayer membrane at different time in the 50 mL aqua regia leaching solution (dilution 50 times) of mobile phone chips. (b) The adsorption ratio of gold ions on the PTL bilayer membrane from the aqua regia leaching solution of the mobile phone chips at different dilution times.

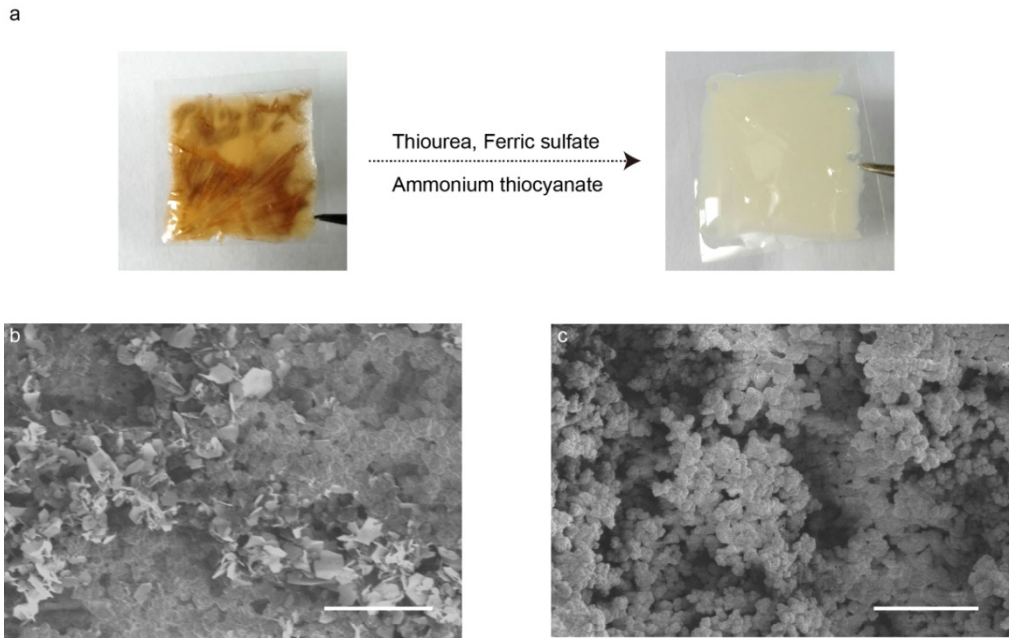

Figure S18. (a) The photograph for the gold-loaded PTL/PET membrane before and after the gold desorption by using the eluent solutions of a combination of thiourea (130 mM), ammonium thiocyanate (780 mM) and ferric sulfate (28 mM). (b-c) The SEM images for the gold-loaded PTL/PET membrane before (b) and after (c) the gold desorption. Scale bars were 10 μm.

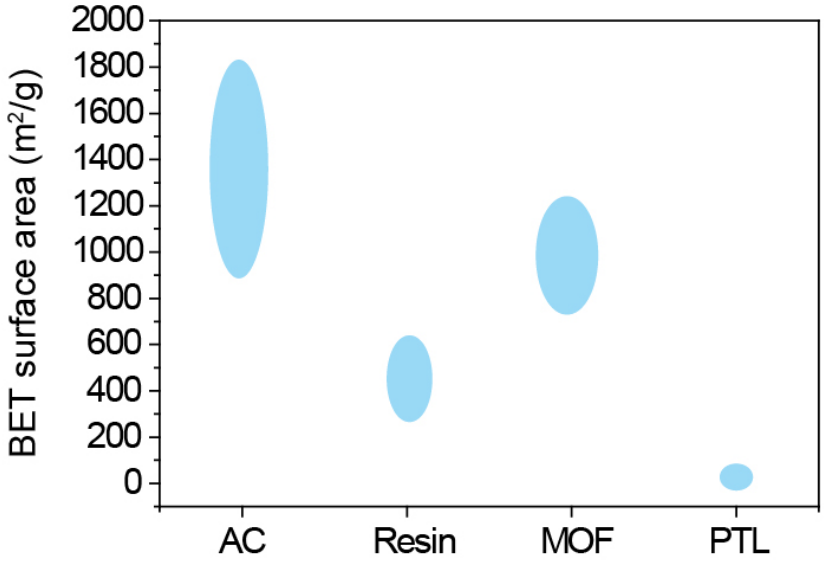

Figure S19. The BET specific surface area of activated carbon (AC),[5] ion exchange resin (Amberlite),[6] metal–organic framework (MOF)[7] and the PTL bilayer membrane. The BET specific surface area data for AC, resin and MOF were taken from the references.

Table S1. A comparison of pseudo-first-order and pseudo-second-order kinetics parameters calculated from the experimental data from **Figure S7**.

Adsorbents	C_0	q_e (exp)	**Pseudo-first-order**		**Pseudo-second-order**		
	ppm		k_1	R_1^2	k_2	q_e	R_2^2
			h^{-1}		g/(mg·h)	mg/g	
PTL	25	61.6	20.38	0.9319	1.0272	62.4	1
	50	121.2	5.202	0.8573	0.0687	129.3	0.9996
	98.5	227.8	1.487	0.9214	0.0084	246.9	0.9997
	196.9	460.6	0.904	0.9182	0.0030	497.5	0.9997
	295.5	699.3	0.885	0.9709	0.0019	746.3	0.9998
	393.9	819.1	0.756	0.8623	0.0008	961.5	0.9956
	492.5	833.7	0.596	0.8727	0.0006	990.1	0.9936
	591.0	870.6	0.658	0.8141	0.0006	1034.1	0.9934
	787.8	906.1	0.814	0.7912	0.0005	1111.1	1

Table S2. Langmuir and Freundlich isotherm adsorption parameters of gold ions adsorbed on the PTL bilayer membrane at different temperatures (referring **Figure S8**).

		Langmuir constants				Freundlich constants		
	T/K	q_m (mg/g)	k_L (L/mg)	R_L^2	R_L	k_F	$1/n$	R_F^2
PTL	283	758.1	0.242	0.9357	0.0042-0.0205	382.6	0.11	0.9947
	310	777.4	0.261	0.8859	0.0039-0.0191	371.4	0.13	0.9982
	333	1034.4	1.118	0.9784	0.0009-0.0045	504.6	0.13	0.9881

Table S3. Thermodynamic parameters of gold ion adsorption on the PTL bilayer membrane.

C_0 (ppm)	ΔH^0 (kJ mol^{-1})	ΔG^0 (kJ mol^{-1})			ΔS^0 (kJ mol^{-1} K^{-1})
		283 K	310 K	333 K	
196.9	45.5	-6.8	-8.1	-16.0	180.8
393.9	23.4	-1.6	-2.5	-5.9	86.7
590.9	12.1	0.2	-0.6	-1.9	41.8
787.8	10.4	1.1	0.6	-0.5	32.5
984.8	7.2	1.7	1.3	0.8	19.2

The thermodynamic parameters such as the change of Gibbs free energy (ΔG^0), enthalpy (ΔH^0) and entropy (ΔS^0) were calculated using the following equations:

$$\Delta G^0 = -RT \ln K_C \qquad (5)$$

$$\Delta G^0 = \Delta H^0 - T\Delta S^0 \qquad (6)$$

where K_C is the distribution coefficient for adsorption and is determined as:

$$K_C = C_a/C_e$$

where C_a is the equilibrium gold ion concentration on the adsorbent (mg/L) and C_e is the equilibrium gold ion concentration in the solution (mg/L).

Table S4. The precious metal-chloro complex species found in aqueous chloride media.[8]

Precious metal	Oxidation state	Ionic radius (pm)	Complexes formed
Pd	+2	86	$[PdCl_4]^{2-}$
	+4	61.5	$[PdCl_6]^{2-}$
Ir	+3	68	$[IrCl_6]^{3-}$
	+4	62.5	$[IrCl_6]^{2-}$
Os	+4	63	$[OsCl_6]^{2-}$
Pt	+2	86	$[PtCl_4]^{2-}$
	+4	62.5	$[PtCl_6]^{2-}$, $[PtCl_5(H_2O)]^{-}$
Ru	+3	68	$[RuCl_6]^{3-}$
	+4	62	$[RuCl_6]^{2-}$, $[Ru_2OCl_8(H_2O)_2]^{2-}$
Rh	+3	66.5	$[RhCl_6]^{3-}$

The selective adsorption for precious metal ion is largely based on the charge-to-size ratio of the chloroanion or the charge density of the species. Since low charged species having smaller hydration shells have higher coulombic interaction with their counter ions than those with larger hydration shells.[9, 10] By this principle, the adsorption capacity for each metal followed the order of $[MCl_6]^{2-}$ > $[MCl_4]^{2-}$ > $[MCl_6]^{3-}$. The adsorption of PTL membrane for platinum group metal followed this order: Pd > Ir > Os > Pt > Ru > Rh. The adsorption capacity of Pd was highest in the platinum group metal. Because at pH 2-3, anionic species such as $[PdCl_4]^{2-}$ and $[PdCl_6]^{2-}$ are predominant and start to appear as the hydroxy complexes such as $Pd(OH)^{+}$, $Pd(OH)_2$ or $[Pd(OH)_4]^{2-}$. $Pd(OH)^{+}$ was possibly bound to carboxyl groups by exchanging with hydrogen ions.[11, 12] The adsorption of other platinum group metal ions on the membrane surface was mainly driven by electrostatic attraction and anion exchange. The adsorption capacity for Ir was higher than Os, since Ir^{3+} ($[IrCl_6]^{3-}$) could readily be oxidized to Ir^{4+} ($[IrCl_6]^{2-}$) and the ionic radius of $[IrCl_6]^{2-}$ was smaller than that of $[OsCl_6]^{2-}$.[13] The $[PtCl_6]^{2-}$ was present in acidic solutions with a moderate excess of chloride ion, which could be exchanged by water to form $[PtCl_5(H_2O)]^{-}$ at pH 2-3 that being weakly adsorbed on the membrane.[14] On the other hand, $[PtCl_4]^{2-}$ showed improved pH stability in aqueous solution compared to $[PtCl_6]^{2-}$. As a result, comparing with the adsorption capacity of Os, a lower adsorption capacity was observed for Pt since the ionic radius of $[PtCl_4]^{2-}$ was larger than that of $[OsCl_6]^{2-}$. In contrast to $[RhCl_6]^{3-}$, the forms for Ru in acidic solution were more complex mainly including $[RhCl_6]^{3-}$, $[RuCl_6]^{2-}$ and $[Ru_2OCl_8(H_2O)_2]^{2-}$. As a result, the adsorption capacity sequence is Pt > Ru > Rh, due to the principle of $[MCl_6]^{2-}$ > $[MCl_4]^{2-}$ > $[MCl_6]^{3-}$ (see above).

References

1 S. Si and T. K. Mandal, *Chem. Eur. J.,* **2007,** *13,* 3160-3168.

2 E. Csapó, D. Ungor, Z. Kele, P. Baranyai, A. Deák, Á. Juhász, L. Janovák and I. Dékány, *Colloid Surface A,* **2017,** *532,* 601-608.

3 H. Wei, Z. Wang, J. Zhang, S. House, Y. G. Gao, L. Yang, H. Robinson, L. H. Tan, H. Xing, C. Hou, I. M. Robertson, J. M. Zuo and Y. Lu, *Nat. Nanotech.,* **2011,** *6,* 93-97.

4 C. Vericat, M. E. Vela, G. Benitez, P. Carro and R. C. Salvarezza, *Chem. Soc. Rev.,* **2010,** *39,* 1805-1834.

5 C. Snyders, S. Bradshaw, G. Akdogan and J. Eksteen, *Hydrometallurgy,* **2014,** *149,* 132-142.

6 N. V. Nguyen, J. C. Lee, S. K. Kim, M. K. Jha, K. S. Chung and J. Jeong, *Gold Bull.,* **2010,** *43,* 200-208.

7 D. T. Sun, N. Gasilova, S. Yang, E. Oveisi and W. Queen, *J. Am. Chem. Soc.,* **2018,** *140,* 16697-16703.

8 F. L. Bernardis, R. A. Grant and D. C. Sherrington, *React. Funct. Polym.,* **2005,** *65*, 205-217.

9 M. Aguilar and J. L. Cortina, *Solvent Extraction and Liquid Membranes,* Taylor & Francis Group, Boca Raton, Florida, USA **2008**.

10 H. V. Ehrlich, T. M. Buslaeva, T. A. Maryutina, Trends in sorption recovery of platinum metals: a critical survey. *Russ. J. Inorg. Chem.* 2017, **62,** 1797.

11 I. D. Vargas, L. E. Macaskie and E. Guibal, *J. Chem. Technol. Biot.,* **2004,** *79,* 49-56.

12 H. Xu, L. Tan, H. Dong, J. He, X. Liu, G. Qiu, Q. He and J. Xie, *RSC Advances,* **2017,** *7,* 32229-32235.

13 J. G. H. Du Preez, C. Viviers, T. Louw, E. Hosten and H. Jonck, *Solvent Extr. Ion Exc.,* **2004,** *22,* 175-188.

14 W. A. Spieker, J. Liu, J. T. Miller, A. J. Kropf and J. R. Regalbuto, *Appl. Catal. A:Gen.,* **2002,** *232***,** 219-235.